On Mixed-Layer Modeling of the Stratocumulus-Topped Marine Boundary Layer

HOWARD P. HANSON

Cooperative Institute for Research in Environmental Sciences, University of Colorado, Boulder, CO 80309

(Manuscript received 11 July 1983, in final form 19 December 1983)

ABSTRACT

Research aircraft measurements of a well-developed marine stratocumulus cloud-topped boundary layer, made in June 1981 off the coast of California, are analyzed using the saturation point method developed by Betts. Estimates of the cloud-top entrainment rate made from the measurements permit construction of a mixing diagram in which the physics of the layer collapse to a single mixing line when diabatic processes and nonstationarity are accounted for. This is possible because the vertically-integrated (mixed-layer) budget equations balance to within measurement uncertainty.

The mixing diagram allows calculation of cloud-top entrainment from the geometry of surface, mixed-layer and above-inversion parcel saturation points (corrected for diabatic processes) and the cloud-top cooling rate. This method, basically an inversion of the thermodynamic budgets, can also be used to calculate surface fluxes. It should be adaptable to routine meteorological data.

While no insight is given into model parameterization of entrainment, it is concluded that, for stratocumulus layers such as the one measured in the data presented here, a mixed-layer model is likely to adequately represent the thermodynamic interactions. However, the data also indicate that the criterion for breakup of a stratocumulus deck used in such models has not been adequately developed.

1. Introduction

The climatically important marine stratocumulus (Sc) cloud regimes that occur over the eastern Pacific west of Peru and California have been the subject of a large number of modeling studies, most of which follow the mixed-layer approach of Lilly (1968). The observational base for many of these studies has been the UCLA cruises in the late 1940s and early 1950s from which a climatology of the Sc deck over the eastern North Pacific was constructed (Neiburger *et al.*, 1961). Wakefield and Schubert (1981), for example, used the Schubert *et al.* (1979) version of the Lilly-type model to simulate the large-scale fields of temperature, moisture and boundary layer depth (as well as heat, moisture, radiative fluxes and cloud thickness), all of which were in general agreement with the Neiburger data. In addition, near the southern limit of the domain of integration (~20°N), Wakefield and Schubert found that moist static energy began to decrease (upward) across the cloud-top inversion, an indication of the possibility of instability of the cloud. This is also in general agreement with observations of the southward extent of the Sc deck.

Such general agreement with large-scale observations represents overall justification of the highly simplified assumptions that comprise the mixed-layer model. Whether the internal details of the model are reasonable or not is a different matter. Various formulations of Lilly's (1968) model, differing in such essentials as the entrainment closure and the treatment of radiative fluxes, give more or less similar results; deciding how to choose among these formulations is, at best, a speculative exercise, in the absence of more detailed measurements.

Recently, Brost *et al.* (1982a,b) presented an exhaustive analysis of aircraft measurements taken west of San Francisco in mid-June 1976. The conditions measured during that experiment were less than ideal for testing the assumptions of a Lilly-type model, due to high wind speeds, the dominance of shear production over buoyancy in the budget of turbulence kinetic energy, and the thin, relatively nonconvective clouds encountered. Nonetheless, several basic assumptions of the mixed-layer modeling approach were shown to hold: nearly well-mixed profiles, below the cloud-top inversion, of conservative thermodynamic variables and approximate linearity of their fluxes; a large ~50 W m^{-2} increase in net (upward) longwave radiation across the cloud top, with an extinction length of the order of the cloud-top excursions; and in-cloud saturation on scales down to several hundred meters. Brost *et al.* (1982b) discussed the need for this last finding to be verified to smaller scales, a difficult measurement problem. One positive aspect of the conditions encountered in 1976 was the low liquid water contents of the clouds, which allowed in-cloud temperature measurements to be taken without the usual sensor wetting problems.

In the present paper, results from one day of another set of research flights, made in late June 1981 to the southwest of San Diego, into the Sc deck over the

eastern North Pacific are presented. During the flight day discussed here, boundary layer winds were weaker ($\lesssim$7 m s^{-1}), the inversion was higher and the cloud deck was substantially thicker with higher liquid water contents than the study above. The flight pattern was designed to obtain detailed sampling in the vertical while drifting with the mean boundary layer wind. A complete description of the experiment, including the aircraft and other flight days is given in a separate report (Hanson, 1982). This paper concentrates on the averaged aspects of the Sc-topped marine boundary layer, with much of the results presented within the framework of saturation point analysis (Betts, 1982a, 1982b). Although the saturation point method is far more general than the mixed-layer formulation, mixed-layer models are highly simplified when analyzed in saturation point coordinates (Betts, 1983).

2. Background

a. *Overview of the research flight*

In late June and early July 1981 the Equatorial Pacific Ocean Climate Studies (EPOCS) program of NOAA sponsored six research flights into the Sc deck to the southwest of San Diego, for which a NOAA/ERL/RFC Lockheed WP-3D Orion was used. The aircraft was equipped with measurement and recording systems for: temperature, water vapor and the three-dimensional wind vector (both slow and fast response); cloud physics, using the Knollenberg FSSP and two-dimensional probes; vertical profiles, using Omega dropwindsondes and aircraft expendable bathythermographs (AXBTs); cloud liquid water, using a (slow response) Johnson-Williams probe; radiative fluxes in a broad infrared and three visible wavebands from pyrgeometers and pyranometers as well as from up-, down- and sideward-looking chopper radiometers; and integrated cloud water, using a microwave radiometer. The gust probe (fast response) system has been described in detail by Bean *et al.* (1976) and other aspects of the P-3 instrumentation are discussed in Bean and Emmanuel (1980) as well as in the experimental report (Hanson, 1982).

This paper makes use, for the most part, of the slow-response (1 s^{-1} samples) measurements of temperature, humidity, liquid water, pressure, radiation, and, to a lesser extent, velocity. Only a small amount of the turbulence data from the gust probe system (40 s^{-1} samples) is used here. Ocean temperatures used here are taken from AXBT surface temperatures. Air temperature measurements were made with a Rosemount thermistor, with a response time of $\sim$1 s and susceptibility to wetting during flight through the relatively dense clouds encountered. Humidity values have been derived from dew-point temperatures measured by a cooled-mirror system. Although accurate, this system has a very slow response ($\gtrsim$5 s) and is also likely affected by cloud water wetting. In-cloud measurements are therefore not stressed here. Radiative flux measurements used come from the Epply 0.3–2.8 μm pyranometers and 3.5–50 μm pyrgeometers (a total of four instruments, one each up-looking and one each down-looking.)

The flight strategy for the day analyzed here was tailored for radiative flux measurements. A series of "racetracks," each consisting of two constant-level averaging runs of about 6 min each, in opposite directions, was made at various altitudes, beginning at 65 m, proceeding up to 2 km and descending again to 65 m. A total of 11 racetracks was made (Fig. 1). The two averaging runs in opposite directions allow aircraft angle-of-attack biases to be averaged out of the solar and infrared flux measurements. They also provide quasi-redundant slow- and fast-response system averages. Throughout the day, the aircraft was maintained as an approximately Lagrangian drifting platform with respect to the mean boundary layer wind. Hence, the changes of the sub-cloud air over about 4 h were measured; these were unexpected and, it will be seen, significant and provide the largest source of analysis uncertainty.

For more complete descriptions of this and the other strategies and the other flight days, the report by Hanson (1982) should be consulted.

b. *Saturation point analysis*

Betts (1982a,b, 1983) has derived and discussed the concept of saturation point analysis of moist thermodynamic processes in the atmosphere; only a brief overview will be given here. In addition, the algorithm used here to calculate the saturation points is derived.

A parcel's saturation pressure is that pressure level to which it must rise (dry adiabatically) or sink (moist

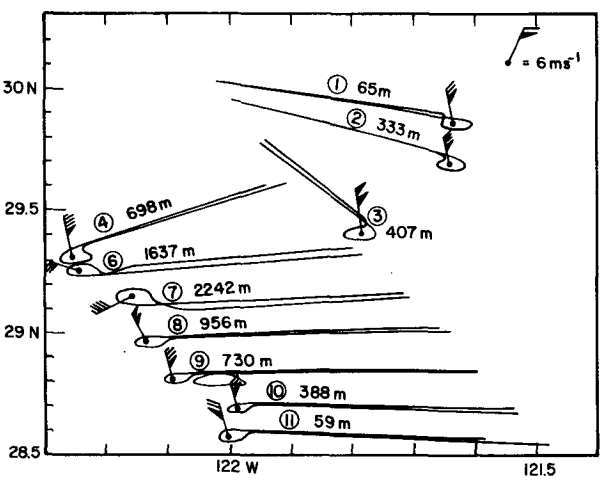

FIG. 1. Racetracks flown in and above the Sc-topped marine boundary layer on 27 June 1981 and racetrack-averaged winds. Racetrack 5 is omitted for clarity; it occurred at $\sim$930 m.

adiabatically) for its total moisture content (which remains unchanged during the rising/sinking) to become just saturated. Therefore, an initially undersaturated parcel of temperature T_0 and mixing ratio $q_0 < q_0^*$ where the asterisk designates saturation properties, rises to its saturation pressure p^* with saturation temperature T^* when

$$q^*(T^*; p^*) = q_0. \tag{1}$$

Its saturation point is then determined by the coordinates (p^*, T^*). Other values may be substituted for these with no loss of generality; here, the coordinates (p^*, θ^*) are used. Conversely, if $q_0 = q_0^*$ and the parcel also contains liquid water with mixing ratio l_0, it must sink to its saturation level, at which point

$$r_0 \equiv q_0^* + l_0 = q^*(T^*; p^*). \tag{2}$$

The process is complicated mathematically, as

$$q^*(T; p) = \frac{0.622e^*(T)}{p - e^*(T)}, \tag{3}$$

where e^*, the saturation vapor pressure, is a very nonlinear function. Saturation points are, however, conveniently found on thermodynamic diagrams.

Betts (1982a) has presented linearized formulas for calculating saturation points. In the present paper, use is made of the above relationships and the resulting transcendental equations are solved iteratively. From the slow-response recording system, values of p_0, T_0, q_0 and l_0 are obtained. (Of course, $l_0 \geq 0$ by definition and this acts as a rectification to separate the implicit dry adiabatic rising from the moist adiabatic sinking.) Then, the parcel "liquid temperature"—that temperature which would result if the liquid water were evaporated at constant pressure—is calculated from

$$T_{l_0} = T_0 \exp\left(-\frac{L}{c_p}\frac{l_0}{T_0}\right), \tag{4}$$

where L is the latent heat of evaporation and c_p is the specific heat of air at constant pressure (both of these are taken as constant here). Below cloud, $T_{l_0} = T_0$. Since liquid *potential* temperature is conserved during either the rising or sinking, it is easy to show that

$$T^* = T_{l_0}(p^*/p_0)^\kappa, \tag{5}$$

where $\kappa = R/c_p$, R being the gas constant. Hence, the saturation pressure can be found by solving

$$r_0 = q^*[T_{l_0}(p^*/p_0)^\kappa; p^*], \tag{6}$$

for p^*. For the profiles shown below, this was accomplished using Newton's method with a 0.5 mb convergence criterion on p^*. The averaged points below were calculated on a hand calculator that has a built-in secant method iteration. Once the saturation pressure is found, the saturation point is given by p^* and $\theta^* = \theta_{l_0} = T_{l_0}(1000/p_0)^\kappa$. Although nonlinear, this formula is smooth enough to converge quite rapidly (typically, with a first guess of p_0, Newton's method requires ≤ 5 steps).

3. 27 June results

a. Vertical structure

The "racetracks" flown on 27 June (Fig. 1) were, as mentioned, displaced such that the aircraft acted approximately as a Lagrangian platform with respect to the boundary layer. Racetrack 5 is omitted from Fig. 1 for clarity; it took place at cloud top and produced unusable gust probe data due to recording system problems. These were corrected and racetrack 8 recorded data at two levels, just above cloud top and just below it, on the two legs. (Slow-response data for racetrack 5 was recorded at two such levels, also.) The large-scale setting for 27 June is shown in Figs. 2. The chart was copied from NWS products; 00Z corresponds to 1800 Pacific Daylight time. The subtropical high is well developed, and the strong E–W pressure gradient

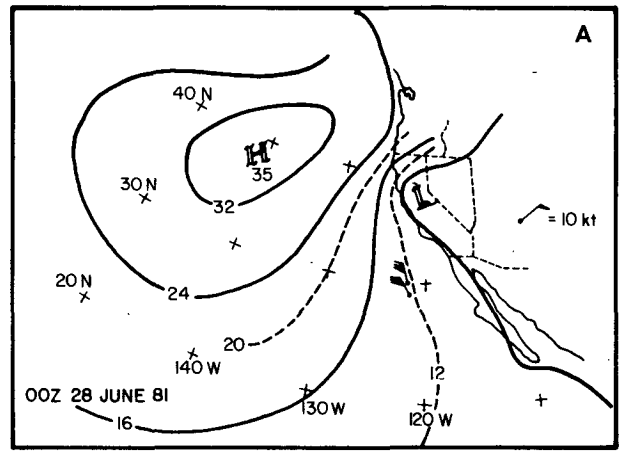

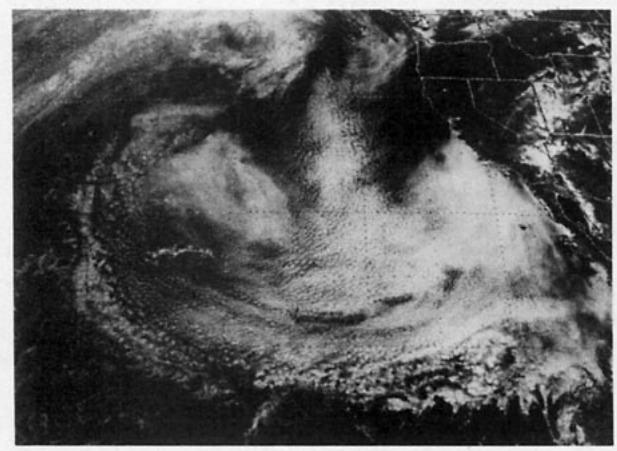

FIG. 2. (a) NWS sea-level analysis 0000 GMT 28 June 1981 and low-level racetrack winds. (b) 1745 GMT visible GOES-West image, 27 June 1981.

between it and the heat low over the Southwest United States is apparent. This has been discussed by Brost *et al.* (1982a). The winds shown in Fig. 2a are the averages of racetracks 1 and 11. Fig. 2b is a morning visible GOES-West image, which depicts a well-developed Sc deck. The 27 June flight occurred within more or less the center of the solid part of the Sc deck, just WNW of Guadeloupe Island (which shows its characteristic lee vortex). Note how the cloud field visibly confirms the NWS flow analysis.

Figures 3a and b are composites of between-racetrack ascents and descents, showing the thermodynamic structure of the marine boundary layer. (In addition to previously defined symbols, θ_e is equivalent potential temperature.) These profiles have been hand-smoothed from the automated plots of the original 1 s^{-1} samples. Also shown are racetrack averages and "filtered" standard deviations. The filtering is a first-pass average through a set of racetrack-leg data after which data points greater than 2 (first-pass) standard deviations were discarded, then the averages recalculated. The dashed section of Fig. 3a is meant to fill in a data gap during a recording computer failure. Fig. 4 shows wind speeds and directions for both the ascent and descent composites.

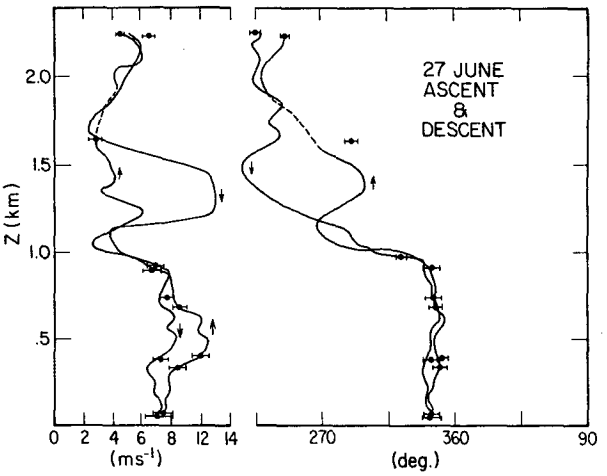

FIG. 4. Composite ascent and descent wind speed and direction profiles and racetrack averages and standard deviations.

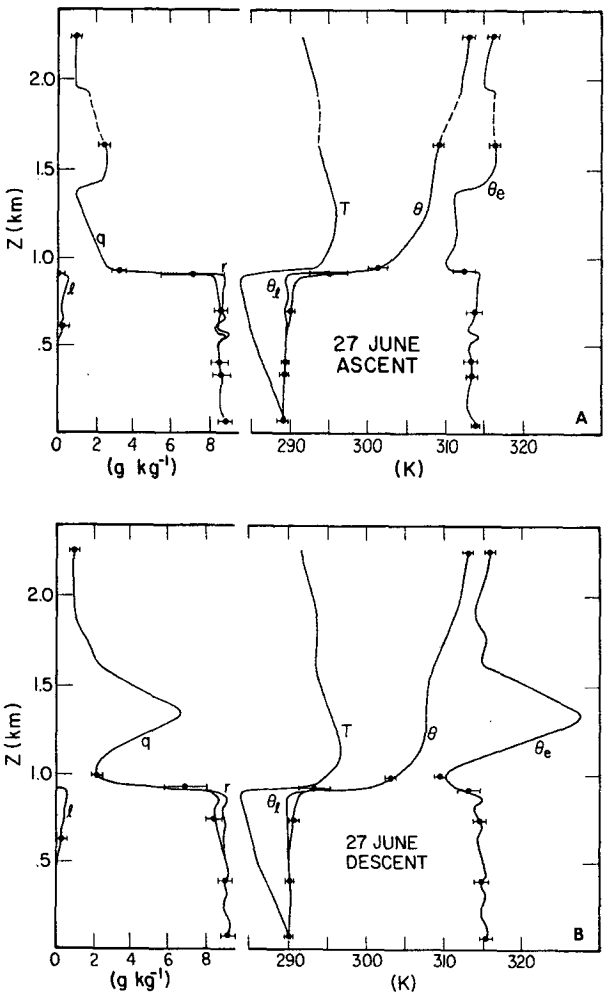

FIG. 3. Composite profiles during (a) ascent and (b) descent of thermodynamic variables. Racetrack averages and standard deviations are also shown.

By far the noisiest quantity in Fig. 3 is the water vapor mixing ratio; the large standard deviations of θ_e are due to this, also. In contrast, the standard deviations of temperature (shown on the θ profile) are far smaller. This is evident because the scales for the two represent the same energy changes, i.e., L/c_p(q-scale) = (T-scale). Similarly, it can be seen that the moisture inversion is somewhat stronger than the temperature inversion, in stark contrast to the Brost *et al.* (1982a) data. Note also the relatively high liquid water mixing ratios—near the cloud top they approach 0.75 g kg^{-1}. The layer structure is nearly well-mixed, although there is moisture stratification on the descent. Whether this is real or an artifact of sensor problems in the cloud is unknown. The basic "mixed-layer" assumption of the Lilly approach seems quite well-founded; this is particularly evident in the constant θ_l profiles, and in the quasi-linear l profiles, both of which are an integral part of such a model. In addition, the inversion is quite sharp in all quantities, ≤50 m thick. Brost *et al.* (1982a) have discussed how a single aircraft penetration overestimates inversion gradients (since the aircraft ascends and descends at a rather shallow angle); even if this were corrected for, the inversions here would be very abrupt.

In contrast to the thermodynamic profiles, the wind structure (Fig. 4) is more variable, although with some tendency for an abrupt change at the inversion level. While the boundary layer wind direction stayed nearly constant throughout the day, the wind speed decelerated, especially in the cloud layer. Variability above the boundary layer is much larger, on long time scales,

in agreement with trade wind results reported by Augstein *et al.* (1973).

The thermodynamically well-mixed nature of the boundary layer is underscored by the saturation pressure profiles in Fig. 5 (the saturation potential temperatures, θ^*, are a repeat of the previous θ_l profiles). The power of the saturation point approach is revealed here: on a thermodynamic diagram the Sc-topped mixed layer reduces to a (somewhat fuzzy) single point. From Fig. 5, it is estimated that the inversion subsided by about 10 m, from ~955 to ~945 m during the time between racetracks 5 and 8, giving $dz_B/dt \approx -0.2$ cm s^{-1}. This value should not be taken too seriously, however, as a 10 m spatial variability in the inversion height could occur as a result of a number of mesoscale processes and there is no guarantee that the cloud was sampled in precisely the same location during the two racetracks. Also from Fig. 5 and the low-level racetrack averages, it is estimated that the boundary layer warmed by ~1.8 K between racetracks 1 and 2 and 10 and 11 (about 4⅓ h), giving $d\theta_{il}/dt = 1.15 \times 10^{-4}$ K s^{-1} (the sub-cloud layer is used for this estimate to eliminate potential sensor wetting errors.) During the same time interval, the boundary layer water content increased by a very small amount (note the decrease of p^* below cloud base from ascent to descent in Fig. 5). From Figs. 3 and the racetracks, $dr/dt = 4.1 \times 10^{-9}$ m s^{-1}. These storage values for θ_l and r are the least precise of the observations used here and are probably within only ±20%. An alternative explanation for the larger subcloud than cloud increases in both q and θ (Figs. 3a and 5) may be that the layer is less well mixed at the end of the descent composite. This would be consistent with the observed sea surface temperature increase from 290.7 K (racetrack 1) to 291.7 K (racetrack 11).

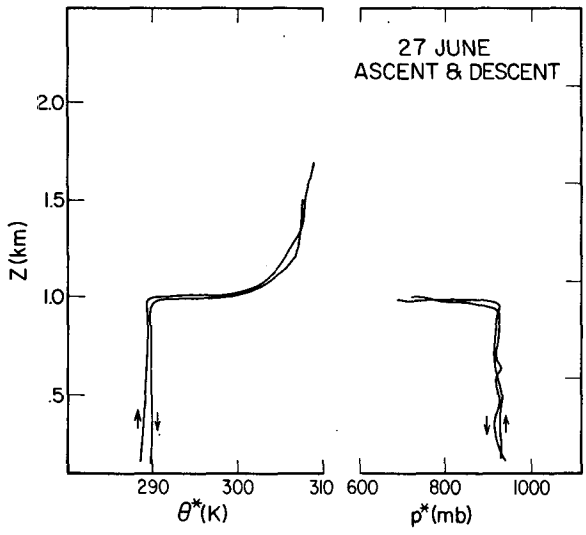

FIG. 5. Composite ascent and descent profiles of saturation potential temperature and saturation pressure.

Details of the radiative flux and cloud microphysical measurements will be discussed elsewhere. The 1981 flights were part of a program to sample cloud effects on radiative transfer in a variety of conditions using a consistent sampling strategy and uniform instrumentation. Several aspects of this flux data are relevant for this paper, however. The net infrared flux was observed to increase very abruptly across 50 or so meters just below the cloud top from near zero to 73 W m^{-2}. One leg of racetracks 5 and 8 each was flown above the inversion and one leg was flown just above the uppermost part of the cloud in the inversion, above the level at which the cloud becomes solid (Figs. 3). The large filtered standard deviations of this leg for racetrack 8 (Fig. 3b) shows this clearly. The net infrared flux difference between these legs, averaged for racetracks 5 and 8, is about 20% of the total; profiles (not shown) indicate that the remainder occurred within a few tens of meters. The net upward infrared flux from the ocean surface was 18 W m^{-2}.

In contrast, the net solar flux difference between the legs of racetracks 5 and 8 was only a small amount of the total absorbed in the cloud, which averaged, based on the above- and below-cloud racetracks, 126 W m^{-2}. The solar flux profiles, while quite noisy, indicate that this absorption occurred over a depth of several hundred meters within the cloud. Hence, while the net boundary layer warming was 71 W m^{-2}, the solar and sub-cloud infrared heating occurred within the well-mixed zone and the cloud-top infrared cooling was confined to a narrow zone just below and within the mean inversion.

The racetrack standard deviations indicate for the radiative fluxes a confidence interval of ~ ±2 W m^{-2}. Below the cloud, of course, the downward solar flux was quite variable ($\sigma \approx 40$ W m^{-2}) due to small-scale inhomogeneities in the cloud thickness. The implied multiple-reflection absorption coefficient for the cloud, $a_c = 11\%$, is within theoretical expectations (e.g., Stephens, 1978a,b).

b. Layer energetics and modeling implications

The qualitative picture of the Sc cloud-topped boundary layer above lends credence to a modeling approach that utilizes a well-mixed vertical structure. It must yet be ascertained whether the internal energetics of the observed cloud are consistent with those implied by a mixed-layer modeling approach. Rather than an attempt at simulation of the 27 June data, this section presents the observed layer energetics using averaged budgets. A simulation remains to be accomplished, complicated enormously by the nonstationarity of the layer and its response to the solar heating. Nor is a detailed turbulence budget constructed. This section addresses the question of whether the vertical averaging implicit in a mixed-layer model aliases processes that significantly affect the layer energetics: Do the mixed layer budgets balance?

In addition to the slow-response data reviewed previously, this section makes use of fast-response data to deduce latent heat fluxes at the surface. These have been obtained from the gust probe recordings and filtered and analyzed in a manner similar to that used by Greenhut and Bean (1981). A linear regression of the latent heat flux averages of racetracks 1–3 (for which the subcloud layer was well-mixed) extrapolated to the surface gives $\rho L\overline{w'r'_S} = 78$ W m^{-2} with a $\pm 10\%$ or so expected error. The inversion jump of r from the subcloud racetracks (r_M) and the above-cloud legs of racetracks 5 and 8 (r_U), is $r_U - r_M = -6.4$ g kg^{-1}, again to within about 10%. The integrated budget equation for the boundary layer water content is

$$z_B\dot{r}_M - \overline{w'r'_S} - w_e(r_U - r_M) = 0, \qquad (7)$$

where $\dot{r}_M \equiv dr_M/dt$; this is used to solve for $w_e = 0.0035$ m s$^{-1} \pm 20\%$. The water budget is essentially a balance of the surface and cloud-top fluxes and the uncertainty regarding the storage term is unimportant. Accepting the rather questionable value of $dz_B/dt = -0.002$ m s^{-1} given above implies a large-scale divergence of 6.1×10^{-6} s^{-1}; neglecting dz_B/dt gives $4.0 \cdot 10^{-6}$ s^{-1}. These are toward the larger values of the Neiburger *et al.* (1961) climatology but are quite reasonable.

The surface-flux term in Eq. (7) can be written

$$\overline{w'r'_S} = v_S(r_S - r_M), \qquad (8)$$

using $q^*(T_S, p_S)$ and the r_M used above gives the surface transfer rate $v_S = 0.0064$ m s^{-1}. From the sea surface temperature and the sub-cloud potential temperature averages, a surface heat flux is

$$\overline{w'\theta'_{lS}} = v_S(\theta_S - \theta_{lM}) \approx 0.0044 \text{ K m s}^{-1}, \qquad (9)$$

(about 5 W m^{-2}). This estimate of the surface heat flux is considered preferable to extrapolation of gust probe measurements (in analogy to the latent heat fluxes) because the heat fluxes measured on the subcloud layer runs were quite small, of the order of the measurement errors. The heat budget, written in terms of θ_l, is

$$z_B\dot{\theta}_{lM} - \overline{w'\theta'_{lS}} - w_e(\theta_{lU} - \theta_{lM}) + (F_B - F_S)/\rho c_p = R_\vartheta, \qquad (10)$$

where $F_B - F_S$ is the radiative flux difference across the layer and R_ϑ is the residual associated with measurement errors or incorrect assumptions. Using the values quoted above gives $R_\vartheta = 0.0004$ K m s^{-1}, about 10% of the smallest (surface flux) term. However, since the largest term here, the storage term, is the least certain, the residual could be as much as about half the entrainment flux term. Table 1 summarizes the budgets. The moisture budget is forced to balance, since it was used to obtain w_e. The small residual of the heat budget is an independent verification of the validity of a mixed layer assumption in this case.

TABLE 1. Mean budgets, Day 178/1981 (units = 10^{-2} m s^{-1} × quantity).

Quantity	Storage	− Surface flux	+ Entrance flux	+ Diabatic	= Residual
r (g kg^{-1})	0.38	2.63	2.25	0	0*
θ_l (K)	10.96	0.44	−4.59	−5.9	0.04

* Moisture budget used to determine w_e.

Saturation point analysis provides a particularly concise, graphical method of presenting these thermodynamic budgets. Fig. 6 shows various saturation points plotted on a tephigram. The above-inversion air (U) has a saturation pressure of ~590 mb since it is so dry; the surface points (S_1, S_2) occur at their actual pressures since they are assumed saturated. The boundary layer values (M_1, M_2) are taken from the averages of racetracks 1–3 and 10 and 11 respectively. The changes of the boundary layer and surface values from points 1 to 2, about 4⅓ h apart, were discussed above and reflect the storage terms and the advection of the layer over warmer water.

Due to the quasi-logarithmic q^*- and θ-scales of a tephigram, mixing of two air parcels occurs along slightly curved lines. The curved line connecting points U and $\bar{S}$ in Fig. 6 is the locus of points $[f\bar{S} + (1-f)U]$ for all $0 \leq f \leq 1$. ($\bar{S}$ is the average of S_1 and S_2.) Curves $\bar{S}$–U'' and $\bar{M}$–U are similarly constructed. In the absence of other processes, mixtures

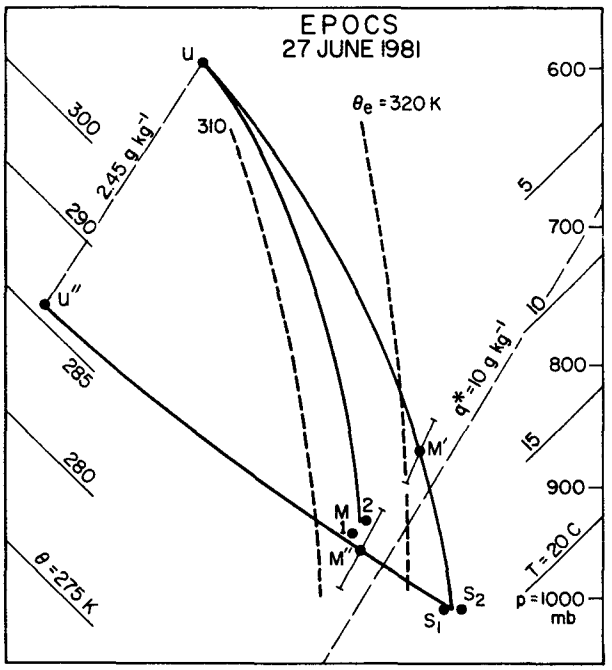

FIG. 6. Mixing diagram plotting saturation points on a tephigram, showing two interpretations of 27 June thermodynamic budgets. See text for explanation.

of surface and upper air parcels fall along the $\bar{S}$–U mixing line.

Returning to the budget equations (7) and (10), it is straightforward to define

$$\left.\begin{aligned} r'_M &= r_M + z_B\dot{r}_M/(w_e + v_S) \\ \theta'_{l_M} &= \theta_{l_M} + (z_B\dot{\theta}_{l_M} + (F_B - F_S)/\rho c_p)/(w_e + v_S) \end{aligned}\right\}, \quad (11)$$

and rewrite the budgets as

$$\begin{aligned} w_e(\theta_{l_U} - \theta'_{l_M}) + v_S(\theta_S - \theta'_{l_M}) &= R_\vartheta \approx 0, \quad (12) \\ w_e(r_U - r'_M) + v_S(r_S - r'_M) &= 0. \end{aligned}$$

Point M' on Fig. 6 is the saturation point for (θ'_{l_M}, r'_M). To the extent that the budgets (7) and (10) balance, Eq. (12) define a mixing line and this is reflected in Fig. 6. The prediction of Betts (1982a, 1983) that accounting for diabatic processes and storage reduces the energetics of the Sc-topped mixed layer to a simple mixing diagram is thus confirmed. This analysis also suggests that assumptions inherent in the mixed-layer approach are valid within measurement error.

The correction factor $\theta'_{l_M} - \theta'_{l_M}$ in Eq. (11) was actually suggested in slightly different form by Betts (1983), based on the interpretation of the role of cloud-top infrared radiation originally used by Lilly (1968) and subsequently adopted in modified form by Deardorff (1976) and Schubert *et al.* (1979). In this interpretation, the fraction of the total infrared cooling that occurs above the *mean* cloud-top height is considered to modify the upper air. Although the observations of Slingo *et al.* (1982) clearly show the radiative cooling to occur within the cloudy air (the cloud droplets, after all, are the entities with high emissivity), some of that cloudy air is continually within the mean inversion. This is a part of the turbulent nature of the entrainment process. Assuming, for simplicity, that all of this cooling is within the inversion (Lilly's, 1968, original approach) suggests a different form of Eq. (11), i.e.,

$$\left.\begin{aligned} r''_M &= r'_M \\ \theta''_{l_M} &= \theta_{l_M} + [z_B\dot{\theta}_{l_M} + (F_{\mathrm{SOL}_B} - F_{\mathrm{SOL}_S})/\rho c_p] \\ &\qquad \times (w_e + v_s)^{-1} \\ \theta''_U &= \theta_U - (F_{\mathrm{IR}_B}/\rho c_p)w_e^{-1} \end{aligned}\right\}, \quad (13)$$

where the infrared (F_{IR}) and solar (F_{SOL}) fluxes have been separated. (The sub-cloud infrared warming is actually included in F_{SOL} here.) This is the modification suggested by Betts (1983). The saturation points U'' and M'' in Fig. 6 correspond to this modification. Since the budgets written using Eq. (13) also take the form of Eq. (12), the mixing line is to be expected and this interpretation of mixed-layer physics is also consistent with the data presented here. From the perspective of the budget equations, then, the precise location of the cloud-top cooling is irrelevant. However, as shown by Deardorff (1976), Stage and Businger (1981) and Randall (1984), parameterized entrainment rates depend strongly on this distinction.

c. Discussion

1) Cloud-top entrainment instability

The mixing line M–U in Fig. 6 represents the actual mixing process between the mixed-layer air and the air above the boundary layer. As discussed by Betts (1982a, 1983), the slope of this line relative to that of moist adiabats (short dashes in Fig. 6) is a measure of the energetics of the mixing process. (The M–U mixing involves saturated air and moist adiabats are relevant. For cases of unsaturated mixing the following discussion applies to dry adiabats.) This is because the slope of constant virtual potential temperature contours under saturated conditions is approximately a constant fraction (~0.9) of the slope of moist adiabats. Any mixing line on a tephigram that slopes to the left of a constant virtual potential contour, then, describes a turbulence kinetic-energy-generating process. For mixing across the top of a stratocumulus (Sc) deck, this is cloud-top entrainment instability (Deardorff, 1980; Randall, 1980). The mixing line M–U in Fig. 6 fulfills this criterion. Another, equivalent, approach is to note that the U–M difference of θ_e is ~ -5.5 K (see also Fig. 3a). Deardorff (1980) showed that cloud-top entrainment instability occurs when $\Delta\theta_e$ is smaller than a critical value that is proportional to the total water difference across the cloud top. In the present case, this critical value is approximately -3.3 K.

Despite the occurrence of this instability, the cloud deck was quite solid on 27 June. Comparison of Fig. 2b with photographs later in the day (not reproduced here) indicates no tendency for the Sc deck to break apart; nor was there any such indication during the course of the research flight. Due to the large-scale flow, of course, the section of the Sc deck measured here was advecting south-southwestward and being replaced by "new" clouds from upstream (referenced to the initial measurement position). However, by the time that any broken structure appears on satellite imagery, the deck has drifted over substantially warmer water, as indicated both by AXBT surveys on other flight days in 1981 and by climatology, hundreds of km away. It seems reasonable to conclude that cloud-top instability does not necessarily lead to breakup of the entire cloud deck. It would, however, be expected to lead to enhanced entrainment (Deardorff, 1980; Stage and Businger, 1981).

2) Inverting the budgets

The simplicity of the mixing diagram (Fig. 6) illustrates the power of the saturation point approach when applied to the Sc-topped marine boundary layer. Points S, M and U were plotted using only thermodynamic

data. The correction factors in Eqs. (11) and (13) used to derive points M', M'' and U'' depend on 1) thermodynamic data at another time (for the storage term) and radiative flux data (which could be calculated, in principle, using a radiative transfer model) and 2) the entrainment rate w_e and the surface transfer rate v_S. Insofar as the points $\bar{S}$, U, U'' form a closed figure, the distance $|U''U|$ is inversely proportional to w_e [see the last part of Eq. (13)] and the ratios

$$\frac{|U''M''|}{|\bar{S}M''|} = \frac{|UM'|}{|\bar{S}M'|} = \frac{v_S}{w_e},$$

[see Eq. (12)], it is possible in principle to use observations of the thermodynamic variables and radiative fluxes to calculate v_S and w_e from diagrams such as Fig. 6.

In practice, the curvature of the mixing lines makes this quite difficult and an easier method is to solve Eqs. (7) and (10)—with $R_\vartheta = 0$ and (8) and (9) for the surface flux term—for v_S and w_e. Since R_ϑ was small, using the present data gives, of course, $w_e = 0.0035$ m s^{-1} and $v_s = 0.0064$ m s^{-1}. The effect of observational uncertainty of $\dot{\theta}_{l_M}$ ($\pm 20\%$) can be calculated, giving ranges of 0.30–0.51 and 0.55–0.88 cm s^{-1} for w_e and v_S respectively. This inversion method is currently being tested with other EPOCS data.

4. Conclusions

Aircraft sampling of a marine Sc deck has produced a dataset that fits well into the framework of a mixed-layer theory. The largest source of measurement uncertainty—the (dominant) storage term in the heat budget—exceeds error sources due to possibly incorrect model assumptions: the mixed-layer forms of the heat budget balances to within that uncertainty. Examining the heat and moisture budgets within Betts' (1982a) saturation point framework provides a very straightforward interpretation of the Sc-topped mixed layer in terms of mixing lines on a thermodynamic diagram. In this regard, in so far as the thermodynamic budgets are concerned, it was shown that the precise location of the infrared cooling at the cloud top is irrelevant. This is not the case, however, for entrainment parameterizations.

The nature of the mixing diagram (Fig. 6) suggests that thermodynamic observations may be used to deduce the cloud-top entrainment rate and the surface transfer rate. Due to the curvature of the mixing lines, this seems most easily accomplished by inverting the budget equations (7) and (10). The $\pm 20\%$ uncertainty in the heat budget storage term produces approximately a (+40, −20)% variability in the entrainment and surface transfer rates with this method. Future experiments can reduce this uncertainty simply by including nonstationarity in their sampling strategies. Extension of this budget inversion technique to more complex boundary layers, e.g., the trade wind planetary boundary layer, which is not well-mixed, involves more sophisticated modeling but also seems feasible.

The Sc deck discussed in this paper was subject to cloud-top entrainment instability yet remained unbroken. This suggests that the generation of turbulence kinetic energy by cloud-top entrainment fluxes may not be sufficient to break up a solid Sc deck: mixing *within* the cloud may be sufficiently stable to damp instabilities at its *top*.

In this regard, it should be borne in mind that this paper has concentrated on one day's measurements; verification of these results by other case studies is necessary before they can be generally accepted. The difficult problem of in-cloud measurements remains and the comments of Brost *et al.* (1982a) regarding alternate measurement platforms are very relevant.

Acknowledgments. Support for the research flights was granted by the Equatorial Pacific Ocean Climate Studies (EPOCS) program, NOAA; principal investigators were E. B. Kraus, V. E. Derr and B. R. Bean. V. E. Derr kindly supplied the radiation data presented here. The NOAA/RFC flight crew, especially E. R. Darby and D. L. Turner, flight director and pilot, are to be congratulated for a remarkable job of handling difficult and sometimes obscure flight-maneuver requests. Discussions with B. A. Albrecht, encouragement from A. K. Betts and data processing assistance from K. D. Hanson facilitated preparation of this paper. The metamorphosis of the paper during revision is credited to comments by J. A. Businger, whose interest is greatly appreciated. Support for analysis and further research for this study have been derived from EPOCS and from NSF Grants ATM-80-23334 and ATM-82-09115.

REFERENCES

Augstein, E., H. Riehl, F. Ostapoff and V. Wagner, 1973: Mass and energy transports in an undisturbed Atlantic trade-wind flow. *Mon. Wea. Rev.*, **101**, 101–111.

Bean, B. R., and C. B. Emmanuel, 1980: Aircraft. *Air-Sea Interaction Instruments and Methods*, F. Dobson, L. Hasse and R. Davis, Eds., Plenum, 571–587.

——, R. O. Gilmer, R. F. Hartman, R. E. McGavin and R. F. Reinking, 1976: Airborne measurement of vertical boundary layer fluxes of water vapor, sensible heat and momentum during GATE. NOAA Tech. Memo. ERL WMPO-36, Washington, DC, 83 pp.

Betts, A. K., 1982a: Saturation point analysis of moist convective overturning. *J. Atmos. Sci.*, **39**, 1484–1505.

——, 1982b: Cloud thermodynamic models in saturation point coordinates. *J. Atmos. Sci.*, **39**, 2182–2191.

——, 1983: Thermodynamics of mixed stratocumulus layers: Saturation point budgets. *J. Atmos. Sci.*, **40**, 2655–2670.

Brost, R. A., D. H. Lenschow and J. C. Wyngaard, 1982a: Marine stratocumulus layers. Part I: Mean conditions. *J. Atmos. Sci.*, **39**, 800–817.

——, J. C. Wyngaard and D. H. Lenschow, 1982b: Marine stratocumulus layers. Part II: Turbulence budgets. *J. Atmos. Sci.*, **39**, 818–836.

Deardorff, J. W., 1976: On the entrainment rate of a stratocumulus-topped mixed layer. *Quart. J. Roy. Meteor. Soc.*, **102,** 563–582.

——, 1980: Cloud-top entrainment instability. *J. Atmos. Sci.*, **37,** 131–147.

Greenhut, G. K., and B. R. Bean, 1981: Aircraft measurements of boundary-layer turbulence over the central Equatorial Pacific Ocean. *Bound.-Layer Meteor.*, **20,** 221–241.

Hanson, H. P., 1982: EPOCS-1981 Summary Data Report: Aircraft measurements of radiation, turbulent transport and profiles in the atmospheric and oceanic boundary layers of the Pacific off California. NOAA Tech. Memo. ERL ESG-1, 157 pp.

Lilly, D. K., 1968: Models of cloud-topped mixed layers under a strong inversion. *Quart. J. Roy. Meteor. Soc.*, **94,** 292–309.

Neiburger, M., D. S. Johnson and C. Chien, 1961: *Studies of the Structure of the Atmosphere over the Eastern Pacific Ocean in Summer. I. The Inversion over the Eastern North Pacific Ocean.* University of California Publications in Meteorology, Los Angeles, 58 pp.

Randall, D. A., 1980: Conditional instability of the first kind upside-down. *J. Atmos. Sci.*, **37,** 125–130.

——, 1984: Buoyant production and consumption of turbulence kinetic energy in cloud-topped mixed layers. *J. Atmos. Sci.*, **41,** 402–413.

Schubert, W. H., J. S. Wakefield, E. J. Steiner and S. K. Cox, 1979: Marine stratocumulus convection. Part I: Governing equations and horizontally homogeneous solutions. *J. Atmos. Sci.*, **36,** 1286–1307.

Slingo, A., R. Brown and C. L. Wrench, 1982: A field study of nocturnal stratocumulus; III. High resolution radiative and microphysical observations. *Quart. J. Roy. Meteor. Soc.*, **108,** 145–165.

Stage, S. A., and J. A. Businger, 1981: A model for entrainment into a cloud-topped marine boundary layer. Part II. Discussion of model behavior and comparison with other models. *J. Atmos. Sci.*, **38,** 2230–2242.

Stephens, G. L., 1978a: Radiation profiles in extended water clouds. I: Theory. *J. Atmos. Sci.*, **35,** 2111–2122.

——, 1978b: Radiation profiles in extended water clouds. II. Parameterization schemes. *J. Atmos. Sci.*, **35,** 2123–2132.

Wakefield, J. S., and W. H. Schubert, 1981: Mixed-layer model simulation of eastern North Pacific stratocumulus. *Mon. Wea. Rev.*, **109,** 1952–1968.